Power Flow Model for Medium-voltage Distribution Systems Considering Measurement and Structure Characteristics

Zhengmei Lu, *Student Member*, *IEEE*, Wei Yan, *Member*, *IEEE*, Dezhi Huang, Junjie Tang, *Member*, *IEEE*, Ferdinanda Ponci, *Senior Member*, *IEEE*, and Antonello Monti, *Senior Member*, *IEEE*

***Abstract*—Medium-voltage distribution systems (MVDSs) mainly consist of a feeder head, lines, distribution transformers, and the equivalent load or power supply interfaced with the distribution transformers. The information of such load or power supply can be measured via the three-wattmeter method (THM) and the two-wattmeter method (TWM). The measurements can be used to perform the control of the power supply and simulate the characteristics of the load, so the models of the load and the power supply need to consider the measurement characteristics. Existing research works on three-phase power flow (PF) just consider the measurement characteristics of THM. Hence, the PF equation of the bus measured via TWM is firstly built. Based on conventional measurements, an accurate and general model of the grounded and ungrounded slack bus is proposed. Furthermore, the influence arising from the connection type and angle shift of distribution transformers on the admittance matrix is considered, and thus a general three-phase transformer model is summarized, which is applicable for all the transformers mentioned herein. Finally, Newton's method is adopted to solve the PF calculation, and the performance of the proposed PF model is demonstrated through designed tests.**

***Index Terms*—Medium-voltage distribution system, three-phase power flow calculation, measurement characteristic, slack bus modeling, distribution transformer.**

I. Introduction

THE medium-voltage distribution system (MVDS) is usually treated as an independent unit for power flow (PF) calculation and application of line loss management in distribution automation systems (DASs). The MVDS is mainly composed of the feeder head, three-phase three-wire distribution lines, distribution transformers, and the equivalent load or power supply interfaced with transformers. In this paper, the bus with fixed power injections is regarded as the equivalent load, and the bus with voltage controllers is regarded as the equivalent power supply. There are various kinds of instruments used for continuous monitoring. The measuring instruments consist of two kinds of principles: the three-wattmeter method (THM) and the two-wattmeter method (TWM). The difference between TWM and THM lies in the wiring and measurements of the measuring instruments. The wiring of the measuring instrument has nothing to do with the internal wiring of the load or power supply, but is related to the line configuration connecting the load or power supply [1]. For the buses in the three-phase three-wire network (TTN), the TWM is selected as the measurement method. The reason is that the neutral point of the bus would be inaccessible. Besides, TWM is effective and low-cost [1]. The point of common coupling (PCC) with distributed energy resources (DERs) or a large capacity load is mostly measured via TWM. TWM obtains power by measuring interphase variables, i. e., phase-to-phase voltage and line currents, rather than the variables in each single phase. The THM is selected for the buses in the three-phase four-wire network (TFN). Whether the voltage, current, or load is balanced, both THM and TWM can accurately measure the voltage, current, and corresponding complex power [1]. In MVDS, there are six types of connections of two-winding transformers: Y/Y, Y/Yn, Y/Δ, Δ/Yn, Δ/Y, and Δ/Δ. The buses on the secondary side of transformers may belong to the TFN, and these buses are measured via THM. Online PF calculation uses measurements and predicted values from measurements as the input. The data transmitted to the supervisory control and data acquisition (SCADA) are regarded as conventional measurements that mostly consist of two different measuring principles. These measurements should be used to build the PF equation of the MVDS in practice.

As an important tool for power systems, the results of PF calculation can provide a theoretical foundation for power loss, status assessment, and secure operation analysis [2], [3]. At present, there are abundant theoretical research works

Manuscript received: January 19, 2023; revised: April 4, 2023; accepted: May 15, 2023. Date of CrossCheck: May 15, 2023. Date of online publication: June 20, 2023.

This work was supported in part by the National Natural Science Foundation of China (No. 52177071).

Z. Lu, W. Yan, and J. Tang (corresponding author) are with State Key Laboratory of Power Transmission Equipment & System Security and New Technology, Chongqing University, Chongqing 400044, China (e-mail: luzmwork@163.com; cquyanwei@cqu.edu.cn; tangjunjie@cqu.edu.cn).

D. Huang is with State Grid Zhejiang Yiwu Power Supply Company, State Grid Zhejiang Electric Power Company, Yiwu 322001, China (e-mail: dezhihwang@126.com).

F. Ponci and A. Monti are with the Institute for Automation of Complex Power Systems of the E.ON Energy Research Center at RWTH Aachen University, Aachen, 52074, Germany, and A. Monti is also with the Digital Energy Fraunhofer FIT, Aachen, 52072, Germany (e-mail: fponci@eonerc. rwth-aachen. de; amonti@eonerc.rwth-aachen.de).

DOI: 10.35833/MPCE.2023.000035

on the three-phase PF model of the asymmetrical system. References [4]-[7] study the three-phase PF model for the ungrounded MV system. The PF equations of the power supply and load in [4]-[7] are built based on the phase-to-ground voltage magnitude and complex power, which are obtained by the phasor measurement units and intelligent electronic devices. In fact, these measuring instruments are rarely installed in the distribution systems. For the hybrid TTN and TFN distribution systems, the measurement characteristics of THM and TWM are not considered together in the PF models [8]-[11]. The PF equations in the salient work [12], [13] are established by the phase-to-neutral complex power and voltage magnitude, which conform to the characteristics of the THM. However, no PF equation in existing references regarding the PF model is applicable to the load or power supply measured via the TWM. Recent studies [14]-[16] propose that a constraint needs to be added to improve the convergence for the ungrounded bus in the TTN, and the constraint is the zero-sequence current equals zero. Reference [14] establishes the PF model of the power supply based on the total active power measured via TWM and the control of three phase-to-phase voltage magnitudes. However, the measurements of TWM and the PF model of the load measured via TWM are neglected in [14]. Considering the measuring characteristics of THM and TWM in MVDS, improved PF equations built for buses measured via TWM are involved in the proposed PF model.

The feeder head is on the secondary side of the HV/MV substation and is generally selected as the slack bus in MVDS. A small resistance is used by the neutral point of the slack bus for grounding, due to the single-phase grounding fault when the load and underground cables are increased. In the current study, the grounding structure is not considered in the slack bus model. The three-phase PF analysis in [17] states that the neutral point should consider its voltage when it is grounded through a resistance, and an improved model is proposed for synchronous machines, generators, or motors. However, this model is not suitable for the slack bus. Moreover, the slack bus in MVDS is affected by the higher-level network and other feeders, and its three-phase voltage magnitude can not be maintained at 1 p.u.. Therefore, the model of the slack bus also needs to consider the measurement characteristics.

In addition, the transformer is a particularly important component in the PF model. In [18], [19], three independent single-phase transformers represent a three-phase transformer, i.e., there is no magnetic coupling among the three phases. There have also been efforts to take into account the influence of interphase coupling. References [20]-[22] make use of the phase-sequence conversion relationship to derive a three-phase transformer model with interphase coupling. Models in [20] and [22] ignore the angle shift relationship. The consideration of connection type in [21] introduces complexity to the angle shift relationship. Therefore, a general transformer model that simultaneously considers the interphase coupling, excitation branches, connection types, and angle shift relationship is derived and summarized. Finally, the innovations of this paper are described as follows.

1) The improved PF equations are built for the equivalent load and equivalent power supply measured via TWM. These equations take the zero-sequence current, phase-to-phase active power, phase-to-phase reactive power, or phase-to-phase voltage magnitude as the inputs of the PF model to reduce the error arising from the measurement modifications.

2) An accurate and general PF model for the slack bus is firstly put forward. Besides, a general model of the three-phase two-winding distribution transformers with six connection types in MVDS is established. It is convenient to implement the above two improvements in practice, which conform to the structure characteristics of MVDS.

3) The development for the PF model of MVDS is achieved. The improved PF equations, the accurate slack bus model, and the general model of transformers are all taken into account in the proposed model, which fully considers the measurement and structure characteristics of MVDS.

II. PF Equations of Equivalent Power Supply and Load Measured via TWM

The measurements as the input of the PF model are used to establish the PF equations of the power supply and load.

The measuring instrument provides the voltage, current, and phase difference between voltage and current according to different measuring circuits, and the corresponding complex power is calculated according to the algorithm of the measuring instrument [1]. The terminal of the measuring instrument determines the corresponding measuring quantity.

A. Principle of TWM

In the TWM measuring circuits, one phase is assigned as the common terminal. Phase c is used as an example to illustrate the principle and derive the PF equations. The corresponding diagram of measuring circuits for TWM is shown in Fig. 1. Let the superscript of the variable represents the phase, and the subscript of the variable represents the bus number. Suppose that $\dot{I}_i^{\beta}$ ($\beta \in \{a,b\}$) is the current injection phasor, and $WT_{\beta c}$ is the sensing element in the measuring instrument. So, the measurement principle can be presented as:

$$\begin{cases} \tilde{S}_i^{ac} = \dot{U}_i^{ac} (\dot{I}_i^{a})^* = (\dot{U}_i^{a} - \dot{U}_i^{c})(\dot{I}_i^{a})^* \\ \tilde{S}_i^{bc} = \dot{U}_i^{bc} (\dot{I}_i^{b})^* = (\dot{U}_i^{b} - \dot{U}_i^{c})(\dot{I}_i^{b})^* \\ \tilde{S}_i^{\Sigma} = \tilde{S}_i^{ac} + \tilde{S}_i^{bc} \end{cases} \tag{1}$$

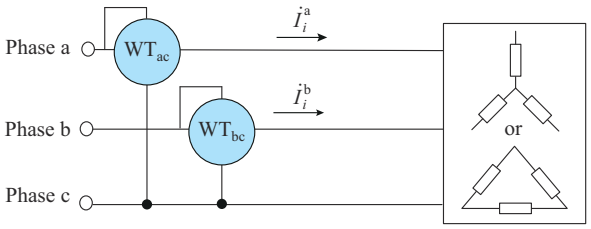

Fig. 1. Diagram of measuring circuits for TWM.

where $\dot{U}_i^{\beta}$ is the phase-to-ground voltage phasor; $\tilde{S}_i^{\Sigma}$ is the total complex power for three phases; and $\tilde{S}_i^{\beta c}$ and $\dot{U}_i^{\beta c}$ are the phase-to-phase complex power and phase-to-phase voltage phasor, respectively. The measurement principle is indepen-

dent of the load (or power supply) wiring. The measurements are taken to perform the controls, and the PF equation can be affected by how the measurements are used. In the next subsections, the PF equations of power supply and load are presented.

B. PF Equations of Power Supply Measured via TWM

The measurements of such an equivalent power supply are phase-to-phase active power and phase-to-phase voltage magnitudes, and the numbers of these two measurements both equal 2. The PF equation, adopting the given measurements as input, can be expressed as:

$$\begin{cases} P_i^{\beta c} = real(\dot{U}_i^{\beta c}(\dot{I}_i^{\beta})^*) = (e_i^{\beta} - e_i^{c}) \sum\limits_{k \in \varphi_i} \sum\limits_{t \in B_p} (G_{ik}^{\beta t} e_k^t - B_{ik}^{\beta t} f_k^t) + \\ \qquad (f_i^{\beta} - f_i^{c}) \sum\limits_{k \in \varphi_i} \sum\limits_{t \in B_p} (G_{ik}^{\beta t} f_k^t + B_{ik}^{\beta t} e_k^t) \\ (U_i^{\beta c})^2 = (e_i^{\beta} - e_i^{c})^2 + (f_i^{\beta} - f_i^{c})^2 \end{cases} \tag{2}$$

where B_p is the set of phases, $B_p = \{a, b, c\}$; $U_i^{\beta c}$ and $P_i^{\beta c}$ are the phase-to-phase voltage magnitude and phase-to-phase active power, respectively; *real*(·) means acquiring the real part; φ_i is the set of all buses (including bus i) connected to bus i; the voltage phasor is presented in a rectangular coordinate system and its real and imaginary parts are represented as e and f, respectively; and $G_{ik}^{\beta t}$ and $B_{ik}^{\beta t}$ are the conductance and susceptance corresponding to the admittance, respectively, which can be obtained from the nodal admittance matrix $\boldsymbol{Y}_{ik}^{\beta t}$.

Except for the slack bus, the zero-sequence current of buses in TTN equals zero. This constraint should be considered in the PF equation as:

$$\begin{cases} \sum\limits_{d \in B_p} \left[\sum\limits_{k \in \varphi_i} \sum\limits_{t \in B_1} (G_{ik}^{dt} e_k^t - B_{ik}^{dt} f_k^t) \right] = 0 \\ \sum\limits_{d \in B_p} \left[\sum\limits_{k \in \varphi_i} \sum\limits_{t \in B_1} (G_{ik}^{dt} f_k^t + B_{ik}^{dt} e_k^t) \right] = 0 \end{cases} \quad B_1 = \{a, b, c, n\} \tag{3}$$

where B_1 represents the set of phases.

The proposed PF equations of the power supply are established based on the constraint that the sum of injection currents equals zero in (3). In addition, the phase-to-phase active power and phase-to-phase voltage magnitudes are taken as the input of PF calculation in (2).

C. PF Equations of Load Measured via TWM

The measurements of such equivalent load are phase-to-phase active power and phase-to-phase reactive power, and the numbers of these two measurements both equal 2. The PF equations, which use the given measurements as input, can be expressed as:

$$\begin{cases} P_i^{\beta c} = real(\dot{U}_i^{\beta c}(\dot{I}_i^{\beta})^*) \\ Q_i^{\beta c} = imag(\dot{U}_i^{\beta c}(\dot{I}_i^{\beta})^*) = -(e_i^{\beta} - e_i^{c}) \sum\limits_{k \in \varphi_i} \sum\limits_{t \in B_p} (G_{ik}^{\beta t} f_k^t + B_{ik}^{\beta t} e_k^t) + \\ \qquad (f_i^{\beta} - f_i^{c}) \sum\limits_{k \in \varphi_i} \sum\limits_{t \in B_p} (G_{ik}^{\beta t} e_k^t - B_{ik}^{\beta t} f_k^t) \end{cases} \tag{4}$$

where *imag*(·) means acquiring the imaginary part; and $Q_i^{\beta c}$ is the phase-to-phase reactive power.

For the load, the proposed PF equations are established based on the constraint that the sum of injection currents equals zero in (3). The phase-to-phase active power and phase-to-phase reactive power are taken as the input of PF calculation in (4).

If phase a or phase b is the common wiring of the meter, the proposed PF equations are still applicable, which only require a simple transformation of the superscript of (1), (2), and (4). When phase a is the common wiring of the meter, the superscripts c and a are changed to a and c, respectively, and $\beta \in \{b,c\}$. When phase b is the common wiring of the meter, the superscripts c and b are changed to b and c, respectively, and $\beta \in \{a,c\}$.

III. Improved Models of Slack Bus and Distribution Transformers Considering Structure Characteristics

The power supply radius and load in MVDS increase, so the utilization of underground cables also increases. Through the resistance, the feeder head needs to be grounded to reduce the occurrence of the single-phase grounding fault. In MVDS, there are six types of connection of two-winding transformers: Y/Y, Y/Yn, Y/Δ, Δ/Yn, Δ/Y, and Δ/Δ. The neutral point voltage of the equivalent load or power supply on the secondary side of Δ/Yn, Y/Yn type transformers can not be ignored.

A. An Accurate and General Model of Slack Bus

The feeder head is generally selected as the slack bus, and it is affected by the higher-level network and other feeders. Its measurements can predict and characterize the control of the slack bus. When the neutral point is grounded through a small resistance, its voltage can not be neglected and the phase-to-neutral voltage magnitude reflects the control model [17]. Furthermore, the voltage measurement of the feeder head is in terms of the phase-to-neutral voltage magnitude, and the three-phase voltage phasor may be unbalanced. In this improved model, the neutral point voltage of the feeder head is considered, and the PF equation of voltage magnitudes is expressed as:

$$(U_s^{dn})^2 = (e_s^d - e_s^n)^2 + (f_s^d - f_s^n)^2 \quad d \in \{a, b, c\} \tag{5}$$

where U_s^{dn} is the phase-to-neutral voltage magnitude; and subscript s represents the slack bus. The voltage angle of phase a is 0°. The voltage angles of phases b and c are −120° and 120°, respectively, which are considered as PF equations as (6).

$$\begin{cases} e_s^b / \cos(-120°) - f_s^b / \sin(-120°) = 0 \\ e_s^c / \cos(120°) - f_s^c / \sin(120°) = 0 \end{cases} \tag{6}$$

For the slack bus, the neutral point current equals the injection currents of three phases. This constraint needs to be taken as PF equations and can be expressed as:

$$\begin{cases} 0 = \sum\limits_{d \in B_p} \sum\limits_{k \in \varphi_s} \sum\limits_{\delta \in B_1} (G_{sk}^{d\delta} e_k^{\delta} - B_{sk}^{d\delta} f_k^{\delta}) - e_s^n G_{ss}^{nn} \\ 0 = \sum\limits_{d \in B_p} \sum\limits_{k \in \varphi_s} \sum\limits_{\delta \in B_1} (G_{sk}^{d\delta} f_k^{\delta} + B_{sk}^{d\delta} e_k^{\delta}) - f_s^n G_{ss}^{nn} \end{cases} \tag{7}$$

where δ represents the set of phases. The slack bus model in [4]-[7] takes the phase-to-ground voltage magnitude and angle as constants, which is only suitable for the ungrounded feeder head. In the improved model, the neutral point voltage and the grounding resistance are set to zeros when the neutral point of the slack bus is ungrounded. As a result, the neutral point current in (7) is not considered and the phase-to-neutral voltage magnitude in (5) equals the phase-to-ground voltage magnitude. For the ungrounded slack bus, the improved model is consistent with other models in [4]-[7] and converts the phase-to-ground voltage phasor of three phases from the polar coordinate system to the rectangular coordinate system through (5) and (6). For the grounded slack bus, the improved model considers the neutral point voltage in (5) and the neutral point current in (7), which is not considered in other models.

The improved model is accurate and general because it is more suitable for the grounded slack bus. Besides, this model considers the measurement and structure characteristics.

B. General Model for Six Types of Distribution Transformer

Aiming at the six connection types of transformers in the MVDS, the general nodal admittance matrix of distribution transformers is presented as:

$$\begin{cases} \begin{bmatrix} \boldsymbol{I}_i \\ \boldsymbol{I}_j \end{bmatrix} = \begin{bmatrix} \boldsymbol{M}\boldsymbol{A}_1 & \boldsymbol{0} \\ \boldsymbol{0} & \boldsymbol{A}_2 \end{bmatrix} \begin{bmatrix} \boldsymbol{Y}_1 + \boldsymbol{Y}_{Nm1} & \boldsymbol{Y}_2 \\ \boldsymbol{Y}_3 & \boldsymbol{Y}_4 + \boldsymbol{Y}_{Nm2} \end{bmatrix} \begin{bmatrix} \boldsymbol{A}_1^{\mathrm{T}}\boldsymbol{M}^{\mathrm{T}} & \boldsymbol{0} \\ \boldsymbol{0} & \boldsymbol{A}_2^{\mathrm{T}} \end{bmatrix} \begin{bmatrix} \boldsymbol{U}_i \\ \boldsymbol{U}_j \end{bmatrix} \\ \boldsymbol{I}_{\mathrm{node}} = [\dot{\boldsymbol{I}}_{\mathrm{node}}^{\mathrm{a}} \quad \dot{\boldsymbol{I}}_{\mathrm{node}}^{\mathrm{b}} \quad \dot{\boldsymbol{I}}_{\mathrm{node}}^{\mathrm{c}} \quad \dot{\boldsymbol{I}}_{\mathrm{node}}^{\mathrm{n}}]^{\mathrm{T}} \\ \boldsymbol{U}_{\mathrm{node}} = [\dot{\boldsymbol{U}}_{\mathrm{node}}^{\mathrm{a}} \quad \dot{\boldsymbol{U}}_{\mathrm{node}}^{\mathrm{b}} \quad \dot{\boldsymbol{U}}_{\mathrm{node}}^{\mathrm{c}} \quad \dot{\boldsymbol{U}}_{\mathrm{node}}^{\mathrm{n}}]^{\mathrm{T}} \end{cases} \tag{8}$$

where $\boldsymbol{I}_{\mathrm{node}}$ and $\boldsymbol{U}_{\mathrm{node}}$ are the current and voltage vectors at bus node i or j; $\boldsymbol{Y}_1$, $\boldsymbol{Y}_2$, $\boldsymbol{Y}_3$, and $\boldsymbol{Y}_4$ are the leakage admittance matrices; $\boldsymbol{Y}_{Nm1}$ and $\boldsymbol{Y}_{Nm2}$ are the excitation admittance matrices; $\boldsymbol{M}$ is the phase shift matrix; and $\boldsymbol{A}_1$ and $\boldsymbol{A}_2$ are the coefficient matrices of bus i and bus j, respectively.

For the bus with Δ connection type, the fourth rows of $\boldsymbol{I}_{\mathrm{node}}$ and $\boldsymbol{U}_{\mathrm{node}}$ are deleted. For the bus with Y connection type, the fourth row of $\boldsymbol{I}_{\mathrm{node}}$ and $\boldsymbol{U}_{\mathrm{node}}$ are zeros.

1) Calculation of Admittance Matrices

The selection rules of $\boldsymbol{Y}_1$, $\boldsymbol{Y}_4$, $\boldsymbol{Y}_{Nm1}$, and $\boldsymbol{Y}_{Nm2}$ are shown in Table I, and the elements in this table are represented as:

$$\begin{cases} \boldsymbol{Y}_{\mathrm{I}} = \begin{bmatrix} \dfrac{\hat{y}+2\check{y}}{3} & \dfrac{\hat{y}-\check{y}}{3} & \dfrac{\hat{y}-\check{y}}{3} \\ \dfrac{\hat{y}-\check{y}}{3} & \dfrac{\hat{y}+2\check{y}}{3} & \dfrac{\hat{y}-\check{y}}{3} \\ \dfrac{\hat{y}-y_1}{3} & \dfrac{\hat{y}-\check{y}}{3} & \dfrac{\hat{y}+2\check{y}}{3} \end{bmatrix} \\ \boldsymbol{Y}_{\Delta} = \begin{bmatrix} \dfrac{2\check{y}}{3} & \dfrac{-\check{y}}{3} & \dfrac{-\check{y}}{3} \\ \dfrac{-\check{y}}{3} & \dfrac{2\check{y}}{3} & \dfrac{-\check{y}}{3} \\ \dfrac{-\check{y}}{3} & \dfrac{-\check{y}}{3} & \dfrac{2\check{y}}{3} \end{bmatrix} \end{cases} \tag{9}$$

For calculating $\boldsymbol{Y}_1$, $\boldsymbol{Y}_2$, $\boldsymbol{Y}_3$, and $\boldsymbol{Y}_4$, $\hat{y}$ and $\check{y}$ are y_{l0} and y_{l1}, respectively. For calculating $\boldsymbol{Y}_{Nm1}$ and $\boldsymbol{Y}_{Nm2}$, $\hat{y}$ and $\check{y}$ are y_{m0} and y_{m1}, respectively. The calculations of y_{l0}, y_{l1}, y_{m0}, and y_{m1} are described in [22]. If one side of the transformer is Δ or Y connection type, $\boldsymbol{Y}_2 = \boldsymbol{Y}_3 = -\boldsymbol{Y}_{\Delta}$; otherwise $\boldsymbol{Y}_2 = \boldsymbol{Y}_3 = -\boldsymbol{Y}_{\mathrm{I}}$.

TABLE I
SELECTION RULES OF $\boldsymbol{Y}_1$, $\boldsymbol{Y}_4$, $\boldsymbol{Y}_{Nm1}$, AND $\boldsymbol{Y}_{Nm2}$

Type of transformer connection	$\boldsymbol{Y}_1$	$\boldsymbol{Y}_4$	$\boldsymbol{Y}_{Nm1}$	$\boldsymbol{Y}_{Nm2}$
Y/Yn	$\boldsymbol{Y}_{\Delta}$	$\boldsymbol{Y}_{\mathrm{I}}$	$1/2\boldsymbol{Y}_{\Delta}$	$1/2\boldsymbol{Y}_{\mathrm{I}}$
Y/Y	$\boldsymbol{Y}_{\Delta}$	$\boldsymbol{Y}_{\Delta}$	$1/2\boldsymbol{Y}_{\Delta}$	$1/2\boldsymbol{Y}_{\Delta}$
Y/Δ	$\boldsymbol{Y}_{\Delta}$	$\boldsymbol{Y}_{\Delta}$	$1/2\boldsymbol{Y}_{\Delta}$	$1/2\boldsymbol{Y}_{\Delta}$
Δ/Yn	$\boldsymbol{Y}_{\Delta}$	$\boldsymbol{Y}_{\mathrm{I}}$	$1/2\boldsymbol{Y}_{\Delta}$	$1/2\boldsymbol{Y}_{\mathrm{I}}$
Δ/Y	$\boldsymbol{Y}_{\Delta}$	$\boldsymbol{Y}_{\Delta}$	$1/2\boldsymbol{Y}_{\Delta}$	$1/2\boldsymbol{Y}_{\Delta}$
Δ/Δ	$\boldsymbol{Y}_{\Delta}$	$\boldsymbol{Y}_{\Delta}$	$1/2\boldsymbol{Y}_{\Delta}$	$1/2\boldsymbol{Y}_{\Delta}$

2) Selection Rules of Coefficient Matrices

The coefficient matrix of the bus with Δ connection type is $\boldsymbol{A}_{\Delta}$; otherwise, it is $\boldsymbol{A}_Y$.

$$\begin{cases} \boldsymbol{A}_{\Delta} = \dfrac{1}{\sqrt{3}\,N} \begin{bmatrix} 1 & -1 & 0 \\ 0 & 1 & -1 \\ -1 & 0 & 1 \end{bmatrix} \\ \boldsymbol{A}_Y = \dfrac{1}{N} \begin{bmatrix} 1 & 0 & 0 \\ 0 & 1 & 0 \\ 0 & 0 & 1 \\ -1 & -1 & -1 \end{bmatrix} \end{cases} \tag{10}$$

where $N = U_{LN}/\sqrt{3}$, and U_{LN} is the rated phase-to-phase voltage magnitude at the bus.

3) Selection Rules of Coefficient Matrices

Table II provides the selection rules of the phase shift matrix $\boldsymbol{M}$. "Connection" means the three phases of the bus on the secondary side of the transformer correspond to phases a, b, and c of the buses on the primary side of the transformer. "+" and "−" represent that the same magnetic polarity of the transformer's two sides is the same and different, respectively. If the bus is Δ connection type, $\boldsymbol{M}$ is directly selected according to Table II; otherwise, $\boldsymbol{M}$ is replaced by $\boldsymbol{M}_Y$.

TABLE II
SELECTION RULE OF $\boldsymbol{M}$

Connection	Type	$\boldsymbol{M}$
b/c/a−	Δ/Y-9, Y/Yn-2, Y/Δ-3, Δ/Yn-9, Y/Y-2, Δ/Δ-2	$-\begin{bmatrix} 0 & 1 & 0 \\ 0 & 0 & 1 \\ 1 & 0 & 0 \end{bmatrix}$
a/b/c−	Δ/Y-5, Y/Yn-6, Y/Δ-7, Δ/Yn-5, Y/Y-6, Δ/Δ-6	$-\begin{bmatrix} 1 & 0 & 0 \\ 0 & 1 & 0 \\ 0 & 0 & 1 \end{bmatrix}$
c/a/b−	Δ/Y-1, Y/Yn-10, Y/Δ-11, Δ/Yn-1, Y/Y-10, Δ/Δ-10	$-\begin{bmatrix} 0 & 0 & 1 \\ 1 & 0 & 0 \\ 0 & 1 & 0 \end{bmatrix}$
c/a/b+	Δ/Y-7, Y/Yn-4, Y/Δ-5, Δ/Yn-7, Y/Y-4, Δ/Δ-4	$\begin{bmatrix} 0 & 0 & 1 \\ 1 & 0 & 0 \\ 0 & 1 & 0 \end{bmatrix}$
b/c/a+	Δ/Y-3, Y/Yn-8, Y/Δ-9, Δ/Yn-3, Y/Y-8, Δ/Δ-8	$\begin{bmatrix} 0 & 1 & 0 \\ 0 & 0 & 1 \\ 1 & 0 & 0 \end{bmatrix}$
a/b/c+	Δ/Y-11, Y/Yn-0, Y/Δ-1, Δ/Yn-11, Y/Y-0, Δ/Δ-0	$\begin{bmatrix} 1 & 0 & 0 \\ 0 & 1 & 0 \\ 0 & 0 & 1 \end{bmatrix}$

$$\boldsymbol{M}_Y=\begin{bmatrix} & \boldsymbol{M} & & 0\\ & & & 0\\ & & & 0\\ 0 & 0 & 0 & 1\end{bmatrix} \tag{11}$$

IV. Solution Method for PF Model of MVDS

The PF model can be solved accurately on the premise that the topology and parameters of MVDS are known and correct, and the proposed model of MVDS is composed of the slack bus, distribution lines, distribution transformers, as well as the equivalent power supply and load. The PF results of the improved PF model can be obtained by means of the original Newton's method [23].

A. Models of Other Components in PF Model

The PF equations of the power supply and load measured via TWM are proposed in Section II, and the models of the slack bus and distribution transformers are improved in Section III. The models of the remaining components are introduced as follows: the PF equations of buses measured via THM take the phase-to-neutral active power, reactive power, and voltage magnitude as the input of the PF model; the PF equations of the load and power supply measured via THM can be found in [12] and [13]; and the line of MVDS is three-phase three-wire and its model can be obtained from [24].

B. Formation of Nodal Balance Equation

Equation (12) contains the nodal balance equations of the equivalent power supply and load measured via the TWM. The deviation of the zero-sequence current at bus i can be divided into real and imaginary parts, which are represented as $\Delta I^0_{i,r}$ and $\Delta I^0_{i,m}$, respectively.

$$\begin{cases}\Delta P_i^{\beta c}=P_{Gi}^{\beta c}-P_{Li}^{\beta c}-real(\dot{U}_i^{\beta c}(\dot{I}_i^{\beta})^*)\\ \Delta Q_i^{\beta c}=Q_{Gi}^{\beta c}-Q_{Li}^{\beta c}-imag(\dot{U}_i^{\beta c}(\dot{I}_i^{\beta})^*)\\ \Delta(U_i^{\beta c})^2=(U_i^{\beta c})^2-(e_i^{\beta}-e_i^{c})^2-(f_i^{\beta}-f_i^{c})^2\\ \Delta I^0_{i,r}=-\sum\limits_{d\in B_p}\left[\sum\limits_{k\in\varphi_i}\sum\limits_{t\in B_1}(G_{ik}^{dt}e_k^t-B_{ik}^{dt}f_k^t)\right]\\ \Delta I^0_{i,m}=-\sum\limits_{d\in B_p}\left[\sum\limits_{k\in\varphi_i}\sum\limits_{t\in B_1}(G_{ik}^{dt}f_k^t+B_{ik}^{dt}e_k^t)\right]\end{cases}\quad \beta\in\{a,b\} \tag{12}$$

The nodal balance equations that are suitable for the equivalent power supply and load measured via the THM and the corresponding Jacobian matrix can be found in [13].

C. Jacobian Matrices of Proposed Model

The real and imaginary parts of the voltage phasor of all buses in a rectangular coordinate system are used as the state variables, which are expressed as (13).

$$\boldsymbol{x}=[e_s^{\delta}\quad f_s^{\delta}\quad e_m^{d}\quad f_m^{d}\quad e_l^{\delta}\quad f_l^{\delta}]\quad \delta\in\{a,b,c,n\},d\in\{a,b,c\} \tag{13}$$

where subscripts m and l represent the bus in the TTN and the bus in the TFN, respectively. The voltage angle of phase a of the slack bus is set to be 0°, i.e., $f_s^a=0$. In order to simplify the derivation of the Jacobian matrices, the state variables include e_m^n and f_m^n. After the Jacobian matrices are formed, the corresponding column vector of f_s^a, e_m^n, and f_m^n should be deleted since these state variables are equal to zeros. The Jacobian matrices for the PF equations measured via TWM and the PF equations of the slack bus are derived in this paper, which can not be found in the existing research works.

1) Jacobian Matrices of PF Equations Measured via TWM

The Jacobian matrix of PF equations measured via TWM is represented as:

$$\boldsymbol{H}_{TMi}=\begin{bmatrix}\boldsymbol{H}_{Tp}(1{:}2,1{:}8) & \boldsymbol{H}_{Tq}(1{:}2,1{:}8)\\ \boldsymbol{H}_{Tz}(1{:}2,1{:}8) & \boldsymbol{H}_{Tu}(1{:}2,1{:}8)\end{bmatrix} \tag{14}$$

where $\boldsymbol{H}_{Tp}$, $\boldsymbol{H}_{Tq}$, $\boldsymbol{H}_{Tz}$, and $\boldsymbol{H}_{Tu}$ are expressed as:

$$\begin{cases}\boldsymbol{H}_{Tp}=\begin{bmatrix}\partial P_i^{\beta c}/\partial e_i^t & \partial P_i^{\beta c}/\partial f_i^t\end{bmatrix}\\ \boldsymbol{H}_{Tq}=\begin{bmatrix}\partial Q_i^{\beta c}/\partial e_i^t & \partial Q_i^{\beta c}/\partial f_i^t\end{bmatrix}\\ \boldsymbol{H}_{Tz}=\begin{bmatrix}\partial \boldsymbol{I}_i^0/\partial e_i^t & \partial \boldsymbol{I}_i^0/\partial f_i^t\end{bmatrix}\\ \boldsymbol{H}_{Tu}=\begin{bmatrix}\partial (U_i^{\beta c})^2/\partial e_i^t & \partial (U_i^{\beta c})^2/\partial f_i^t\end{bmatrix}\end{cases}\quad t\in\{a,b,c,n\} \tag{15}$$

where $\boldsymbol{I}_i^0$ denotes the deviation of the zero-sequence current, and it is divided into two parts which can be represented as $[\Delta I^0_{i,r},\Delta I^0_{i,m}]^{\mathrm{T}}$. And the size of matrices $\boldsymbol{H}_{Tp}$, $\boldsymbol{H}_{Tq}$, $\boldsymbol{H}_{Tz}$, and $\boldsymbol{H}_{Tu}$ is 2×8.

1) For state variables of bus i itself

$$\boldsymbol{H}_{Tp,i}=\begin{bmatrix}\psi_i^{aa} & \psi_i^{ab} & \psi_i^{ac} & 0 & \zeta_i^{aa} & \zeta_i^{ab} & \zeta_i^{ac} & 0\\ \psi_i^{ba} & \psi_i^{bb} & \psi_i^{bc} & 0 & \zeta_i^{ba} & \zeta_i^{bb} & \zeta_i^{bc} & 0\end{bmatrix} \tag{16}$$

where ψ and ζ can be derived as (17) and (18).

$$\begin{cases}\psi_i^{\beta\beta}=\sum\limits_{k\in\varphi_i}\sum\limits_{l\in B_p}(G_{ik}^{\beta l}e_k^l-B_{ik}^{\beta l}f_k^l)+G_{ii}^{\beta\beta}(e_i^{\beta}-e_i^{c})+B_{ii}^{\beta\beta}(f_i^{\beta}-f_i^{c})\\ \psi_i^{\beta_1\beta_2}=G_{ii}^{\beta_1\beta_2}(e_i^{\beta_1}-e_i^{c})+B_{ii}^{\beta_1\beta_2}(f_i^{\beta_1}-f_i^{c})\\ \psi_i^{\beta c}=-\sum\limits_{k\in\varphi_i}\sum\limits_{l\in B_p}(G_{ik}^{\beta l}e_k^l-B_{ik}^{\beta l}f_k^l)+G_{ii}^{\beta c}(e_i^{\beta}-e_i^{c})+B_{ii}^{\beta c}(f_i^{\beta}-f_i^{c})\end{cases} \tag{17}$$

$$\begin{cases}\zeta_i^{\beta\beta}=\sum\limits_{k\in\varphi_i}\sum\limits_{l\in B_p}(G_{ik}^{\beta l}f_k^l+B_{ik}^{\beta l}e_k^l)-B_{ii}^{\beta\beta}(e_i^{\beta}-e_i^{c})+G_{ii}^{\beta\beta}(f_i^{\beta}-f_i^{c})\\ \zeta_i^{\beta_1\beta_2}=-B_{ii}^{\beta_1\beta_2}(e_i^{\beta_1}-e_i^{c})+G_{ii}^{\beta_1\beta_2}(f_i^{\beta_1}-f_i^{c})\\ \zeta_i^{\beta c}=-\sum\limits_{k\in\varphi_i}\sum\limits_{l\in B_p}(G_{ik}^{\beta l}f_k^l+B_{ik}^{\beta l}e_k^l)-B_{ii}^{\beta c}(e_i^{\beta}-e_i^{c})+G_{ii}^{\beta c}(f_i^{\beta}-f_i^{c})\end{cases} \tag{18}$$

where β_1 and β_2 belong to β, and $\beta_1\neq\beta_2$.

$$\boldsymbol{H}_{Tq,i}=\begin{bmatrix}\mu_i^{aa} & \mu_i^{ab} & \mu_i^{ac} & 0 & \eta_i^{aa} & \eta_i^{ab} & \eta_i^{ac} & 0\\ \mu_i^{ba} & \mu_i^{bb} & \mu_i^{bc} & 0 & \eta_i^{ba} & \eta_i^{bb} & \eta_i^{bc} & 0\end{bmatrix} \tag{19}$$

where μ and η can be derived as (20) and (21).

$$\begin{cases}\mu_i^{\beta\beta}=-\sum\limits_{k\in\varphi_i}\sum\limits_{l\in B_p}(G_{ik}^{\beta l}f_k^l+B_{ik}^{\beta l}e_k^l)-B_{ii}^{\beta\beta}(e_i^{\beta}-e_i^{c})+G_{ii}^{\beta\beta}(f_i^{\beta}-f_i^{c})\\ \mu_i^{\beta_1\beta_2}=-B_{ii}^{\beta_1\beta_2}(e_i^{\beta_1}-e_i^{c})+G_{ii}^{\beta_1\beta_2}(f_i^{\beta_1}-f_i^{c})\\ \mu_i^{\beta c}=\sum\limits_{k\in\varphi_i}\sum\limits_{l\in B_p}(G_{ik}^{\beta l}f_k^l+B_{ik}^{\beta l}e_k^l)-B_{ii}^{\beta c}(e_i^{\beta}-e_i^{c})+G_{ii}^{\beta c}(f_i^{\beta}-f_i^{c})\end{cases} \tag{20}$$

$$\begin{cases}\eta_i^{\beta\beta}=\sum\limits_{k\in\varphi_i}\sum\limits_{l\in B_p}(G_{ik}^{\beta l}e_k^l-B_{ik}^{\beta l}f_k^l)-G_{ii}^{\beta\beta}(e_i^\beta-e_i^{\mathrm{c}})-B_{ii}^{\beta\beta}(f_i^\beta-f_i^{\mathrm{c}})\\ \eta_i^{\beta_1\beta_2}=-G_{ii}^{\beta_1\beta_2}(e_i^{\beta_1}-e_i^{\mathrm{c}})-B_{ii}^{\beta_1\beta_2}(f_i^{\beta_1}-f_i^{\mathrm{c}})\\ \eta_i^{\beta\mathrm{c}}=-\sum\limits_{k\in\varphi_i}\sum\limits_{l\in B_p}(G_{ik}^{\beta l}e_k^l-B_{ik}^{\beta l}f_k^l)-G_{ii}^{\beta\mathrm{c}}(e_i^\beta-e_i^{\mathrm{c}})-B_{ii}^{\beta\mathrm{c}}(f_i^\beta-f_i^{\mathrm{c}})\end{cases}\tag{21}$$

$$\boldsymbol{H}_{Tz,i}(1{:}2,1{:}3)=\begin{bmatrix}\partial I_{i,r}^0/\partial e_i^d\\ \partial I_{i,m}^0/\partial e_i^d\end{bmatrix}=\begin{bmatrix}\sum\limits_{l\in B_p}G_{ii}^{ld}\\ \sum\limits_{l\in B_p}B_{ii}^{ld}\end{bmatrix}\quad d\in\{\mathrm{a},\mathrm{b},\mathrm{c}\}\tag{22}$$

$$\boldsymbol{H}_{Tz,i}(1{:}2,5{:}7)=\begin{bmatrix}\partial I_{i,r}^0/\partial f_i^d\\ \partial I_{i,m}^0/\partial f_i^d\end{bmatrix}=\begin{bmatrix}\sum\limits_{l\in B_p}(-B_{ii}^{ld})\\ \sum\limits_{l\in B_p}G_{ii}^{ld}\end{bmatrix}\quad d\in\{\mathrm{a},\mathrm{b},\mathrm{c}\}\tag{23}$$

$$\boldsymbol{H}_{Tu,i}(1{:}2,1{:}8)=[\partial(U_i^{\beta\mathrm{c}})^2/\partial e_i^d\ \ \partial(U_i^{\beta\mathrm{c}})^2/\partial f_i^d]=[\boldsymbol{\rho}_1\ \ 0\ \ \boldsymbol{\rho}_2\ \ 0]\tag{24}$$

where $\boldsymbol{\rho}_1$ and $\boldsymbol{\rho}_2$ can be determined according to (25).

$$\begin{cases}\boldsymbol{\rho}_1=\begin{bmatrix}2(e_i^{\mathrm{a}}-e_i^{\mathrm{c}}) & 0 & -2(e_i^{\mathrm{a}}-e_i^{\mathrm{c}})\\ 0 & 2(e_i^{\mathrm{b}}-e_i^{\mathrm{c}}) & -2(e_i^{\mathrm{b}}-e_i^{\mathrm{c}})\end{bmatrix}\\ \boldsymbol{\rho}_2=\begin{bmatrix}2(f_i^{\mathrm{a}}-f_i^{\mathrm{c}}) & 0 & -2(f_i^{\mathrm{a}}-f_i^{\mathrm{c}})\\ 0 & 2(f_i^{\mathrm{b}}-f_i^{\mathrm{c}}) & -2(f_i^{\mathrm{b}}-f_i^{\mathrm{c}})\end{bmatrix}\end{cases}\tag{25}$$

2) For state variables of other bus j except for bus i

The Jacobian matrices for the state variables of the other bus j except for bus i are represented as (26)-(29).

$$\boldsymbol{H}_{Tp,j}=\begin{bmatrix}\partial P_i^{\beta\mathrm{c}}/\partial e_i^\delta\\ \partial P_i^{\beta\mathrm{c}}/\partial f_i^\delta\end{bmatrix}^{\mathrm{T}}=\begin{bmatrix}G_{ij}^{\beta\delta}(e_i^\beta-e_i^{\mathrm{c}})+B_{ij}^{\beta\delta}(f_i^\beta-f_i^{\mathrm{c}})\\ -B_{ij}^{\beta\delta}(e_i^\beta-e_i^{\mathrm{c}})+G_{ij}^{\beta\delta}(f_i^\beta-f_i^{\mathrm{c}})\end{bmatrix}^{\mathrm{T}}\tag{26}$$

$$\boldsymbol{H}_{Tq,j}=\begin{bmatrix}\partial Q_i^{\beta\mathrm{c}}/\partial e_i^\delta\\ \partial Q_i^{\beta\mathrm{c}}/\partial f_i^\delta\end{bmatrix}^{\mathrm{T}}=\begin{bmatrix}B_{ij}^{\beta\delta}[-(e_i^\beta-e_i^{\mathrm{c}})]+G_{ij}^{\beta\delta}(f_i^\beta-f_i^{\mathrm{c}})\\ G_{ij}^{\beta\delta}[-(e_i^\beta-e_i^{\mathrm{c}})]-B_{ij}^{\beta\delta}(f_i^\beta-f_i^{\mathrm{c}})\end{bmatrix}^{\mathrm{T}}\tag{27}$$

$$\boldsymbol{H}_{Tz,j}=\begin{bmatrix}\partial I_{i,r}^0/\partial e_i^\delta & \partial I_{i,r}^0/\partial f_i^\delta\\ \partial I_{i,m}^0/\partial e_i^\delta & \partial I_{i,m}^0/\partial f_i^\delta\end{bmatrix}=\begin{bmatrix}\sum\limits_{l\in B_p}G_{ij}^{l\delta} & \sum\limits_{l\in B_p}-B_{ij}^{l\delta}\\ \sum\limits_{l\in B_p}B_{ij}^{l\delta} & \sum\limits_{l\in B_p}G_{ij}^{l\delta}\end{bmatrix}\tag{28}$$

$$\boldsymbol{H}_{Tu,j}=\boldsymbol{0}_{2\times8}\tag{29}$$

2) Jacobian Matrices of PF Equations of Slack Bus

$$\boldsymbol{H}_{Si}=[\boldsymbol{H}_{SiI}(1{:}2,1{:}8)\quad\boldsymbol{H}_{Si\theta}(1{:}2,1{:}8)]\tag{30}$$

where $\boldsymbol{H}_{SiI}=[\partial\boldsymbol{I}_s^n/\partial e_i^t,\partial\boldsymbol{I}_s^n/\partial f_i^t]$, $\boldsymbol{I}_s^n$ is the current phasor of the neutral point, and it is divided into two real parts as $\Delta I_{s,r}^{\mathrm{n}}$ and $\Delta I_{s,m}^{\mathrm{n}}$; and $\boldsymbol{H}_{Si\theta}=[\partial{\theta_s}^\beta/\partial e_i^t,\partial{\theta_s}^\beta/\partial f_i^t]$ ($\beta\in\{\mathrm{b},\mathrm{c}\}$).

1) For state variables of the slack bus (s) itself

$$\boldsymbol{H}_{SiL,s}(1{:}2;1{:}4)=\begin{bmatrix}\sum\limits_{t\in B_p}G_{ss}^{t\mathrm{a}} & \sum\limits_{t\in B_p}G_{ss}^{t\mathrm{b}} & \sum\limits_{t\in B_p}G_{ss}^{t\mathrm{c}} & -G_{ss}^{\mathrm{nn}}\\ \sum\limits_{t\in B_p}B_{ss}^{t\mathrm{a}} & \sum\limits_{t\in B_p}B_{ss}^{t\mathrm{b}} & \sum\limits_{t\in B_p}B_{ss}^{t\mathrm{c}} & 0\end{bmatrix}\tag{31}$$

$$\boldsymbol{H}_{SiL,s}(1{:}2;5{:}8)=\begin{bmatrix}-\sum\limits_{t\in B_p}B_{ss}^{t\mathrm{a}} & -\sum\limits_{t\in B_p}B_{ss}^{t\mathrm{b}} & -\sum\limits_{t\in B_p}B_{ss}^{t\mathrm{c}} & 0\\ \sum\limits_{t\in B_p}G_{ss}^{t\mathrm{a}} & \sum\limits_{t\in B_p}G_{ss}^{t\mathrm{b}} & \sum\limits_{t\in B_p}G_{ss}^{t\mathrm{c}} & -G_{ss}^{\mathrm{nn}}\end{bmatrix}\tag{32}$$

$$\begin{cases}\boldsymbol{H}_{Si\theta,s}(1,2)=1/\cos(-120^\circ)\\ \boldsymbol{H}_{Si\theta,s}(1,6)=-1/\sin(-120^\circ)\\ \boldsymbol{H}_{Si\theta,s}(2,3)=1/\cos(120^\circ)\\ \boldsymbol{H}_{Si\theta,s}(2,7)=-1/\sin(120^\circ)\end{cases}\tag{33}$$

where the remaining elements of $\boldsymbol{H}_{Si\theta,s}$ are zeros.

2) For state variables of the other bus except for bus s

$$\boldsymbol{H}_{SiL,i}(1{:}2;1{:}4)=\begin{bmatrix}\sum\limits_{t\in B_p}G_{si}^{t\mathrm{a}} & \sum\limits_{t\in B_p}G_{si}^{t\mathrm{b}} & \sum\limits_{t\in B_p}G_{si}^{t\mathrm{c}} & 0\\ \sum\limits_{t\in B_p}B_{si}^{t\mathrm{a}} & \sum\limits_{t\in B_p}B_{si}^{t\mathrm{b}} & \sum\limits_{t\in B_p}B_{si}^{t\mathrm{c}} & 0\end{bmatrix}\tag{34}$$

$$\boldsymbol{H}_{SiL,i}(1{:}2;5{:}8)=\begin{bmatrix}-\sum\limits_{t\in B_p}B_{si}^{t\mathrm{a}} & -\sum\limits_{t\in B_p}B_{si}^{t\mathrm{b}} & -\sum\limits_{t\in B_p}B_{si}^{t\mathrm{c}} & 0\\ \sum\limits_{t\in B_p}G_{si}^{t\mathrm{a}} & \sum\limits_{t\in B_p}G_{si}^{t\mathrm{b}} & \sum\limits_{t\in B_p}G_{si}^{t\mathrm{c}} & 0\end{bmatrix}\tag{35}$$

$$\boldsymbol{H}_{Si\theta,s}(1{:}2,1{:}8)=\boldsymbol{0}_{2\times8}\tag{36}$$

D. Effectiveness Analysis of Improved Model

The solvability and effectiveness analysis of the improved PF method is described below.

1) For the equivalent power supply measured via TWM, there are six real equations in (2) and (3), and six state variables at the corresponding bus.

2) For the equivalent load measured via TWM, there are six real number equations in (3) and (4), and six state variables at the corresponding bus.

3) For the buses (equivalent power supply or load) measured via THM, there are eight real equations in [7] and eight state variables at the corresponding bus.

4) For the slack bus, there are seven real equations in (5), (6), and (7), and seven state variables at the corresponding bus.

The number of the above power flow equations for the power supply and load is identical to the number of state variables that are covered in (13), so the improved PF model herein can be solvable in theory, if and only if the topology and system parameters are available and correct.

V. Results and Discussion

A. Effect on PF Results of Transformer Model

The IEEE 4-bus (12.47 kV/4.16 kV) system is a standard system, and it is selected especially to verify different transformer models [13]. The structure of this IEEE 4-bus system is shown in Fig. 2, and its detailed parameters can be accessible in [13]. Three transformer models are used to calculate the PF results under symmetrical and asymmetrical loads.

1) Model I: the shunt branch and the interphase coupling are neglected in this transformer model [18].

2) Model II: the interphase coupling is considered but the shunt branch and clock number are neglected in this transformer model [20].

3) Model III: the improved model in this paper accounts for interphase coupling, excitation branches, connection types, and clock number.

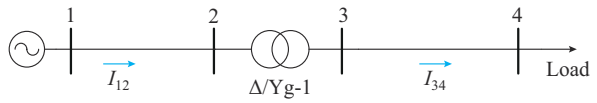

Fig. 2. Structure of IEEE 4-bus system.

The PF results under symmetrical and asymmetrical loads are shown in Table III and IV, respectively. Specifically, Models I and II use the matrix ***M*** proposed in this paper to realize the angle shift conversion which is not considered in [18] and [20].

TABLE III
PF RESULT UNDER SYMMETRICAL LOADS

Bus	Phase	Model I		Model II		Model III	
		U (kV)	θ (°)	U (kV)	θ (°)	U (kV)	θ (°)
2	a	7.109	–0.29	7.110	–0.21	7.112	–0.17
	b	7.130	120.35	7.132	–120.36	7.131	–120.36
	c	7.127	119.60	7.124	119.56	7.123	119.59
3	a	2.249	–34.73	2.250	–33.78	2.252	–33.02
	b	2.265	–153.72	2.263	–153.40	2.259	–153.42
	c	2.253	86.07	2.260	86.33	2.259	86.37
4	a	1.927	–39.37	1.920	–39.07	1.923	–39.07
	b	2.056	–158.62	2.054	–158.31	2.048	–158.31
	c	1.978	80.55	1.986	80.84	1.987	80.85
Power loss (MW)		0.5684		0.5698		0.5723	

TABLE IV
PF RESULT UNDER ASYMMETRICAL LOADS

Bus	Phase	Model I		Model II		Model III	
		U (kV)	θ (°)	U (kV)	θ (°)	U (kV)	θ (°)
2	a	7.109	–0.30	7.125	–0.02	7.125	–0.10
	b	7.119	–120.16	7.154	–120.32	7.153	–120.41
	c	7.115	119.55	7.114	119.59	7.117	119.61
3	a	2.290	–33.59	2.264	–33.36	2.244	–33.39
	b	2.262	–152.10	2.305	–151.89	2.334	–151.80
	c	2.214	85.77	2.243	86.12	2.253	86.06
4	a	2.157	–41.96	1.996	–41.45	1.944	–41.66
	b	1.936	–152.91	2.248	–152.72	2.342	–152.61
	c	1.850	80.55	1.860	80.85	1.863	80.84
Power loss (MW)		0.4721		0.4752		0.4776	

According to the results in the tables, the conclusions are drawn below.

In the condition of symmetrical loads, it can be seen that the calculation results of Model I are quite different from those of Model III. When the load is asymmetric, the difference among the three models is more evident. The maximum voltage magnitude difference between Model I and Model II is 0.312 kV, and the difference in power loss between Model I and Model III is 5.5 kW. This phenomenon demonstrates that interphase coupling has a significant impact on power flow calculation and is very critical for power loss analysis in practical engineering. Although the voltage magnitude difference between Model II and Model III is small, the influence of the shunt branches and the connection type on PF calculation will become larger with the increase of load asymmetry. The voltage angle of each bus conforms to the corresponding angle shift of the transformer type Δ/Yn-1 through the matrix ***M***. The PF results of Model III are more accurate compared with the other models since the effect of connection type on the nodal admittance matrix and interphase coupling are considered in Model III.

B. Performance Test with Different Influencing Factors

1) Test System

A test system of MVDS is designed based on the IEEE 34-bus system [25]. Figure 3 is a single-line diagram of the modified IEEE 34-bus test system. The test conditions and measurements are shown in Appendix A and the parameters of the test system is summarized in Table V.

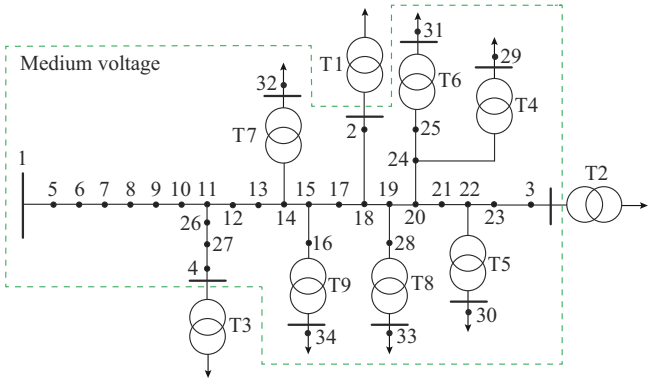

Fig. 3. Single-line diagram of modified IEEE 34-bus test system.

TABLE V
PARAMETERS OF MODIFIED IEEE 34-BUS TEST SYSTEM

Element	System parameter
Slack bus	Bus 1
Grounding resistance of slack bus	20 Ω
Bus in TFN	Buses 29-34
Bus in TTN	Buses 2-28
Blue transformer measured via THM	Δ/Yn-1
Red transformer measured via TWM	Structure and loss are ignored
Equivalent load	Buses 2, 3, 29-34
Equivalent power supply	Bus 4
Connection buses	Buses 5-28

For illustrating the practicality and characteristics of the proposed PF model, two methods proposed in this paper and two commonly used methods in other references are selected for comparison. The model parameters of the four methods are shown in Table VI. The input of the PF equation in the current research works is not based on the measurement of both THM and TWM. When the methods of other references are used, the actual measurements of TWM and THM need to be modified as (37) and (38), respectively.

TABLE VI
MODEL PARAMETERS OF FOUR METHODS

Method	Structure	TWM PF equation	THM PF equation	Slack bus model	Transformer model	Calculation algorithm	Three-phase power flow model
I	Hybrid system	Actual	Actual	Proposed model	Model III	Newton's method	This paper
II	Hybrid system	Actual	Actual	[6]	Model III	Newton's method	This paper
III	Hybrid system	Modified	Actual	[6]	Model III	Newton's method	[10]
IV	Three-phase three-wire	Modified	Modified	[6]	Fixed loss	Newton's method	[4]

$$\begin{cases} \bar{P}_i^d \approx (P_i^{ac} + P_i^{ac})/3 \\ \bar{Q}_i^d \approx (Q_i^{ac} + Q_i^{ac})/3 \\ \bar{V}_i^d = \sqrt{3}\,(V_i^{ac} + V_i^{bc})/2 \end{cases} \tag{37}$$

$$\begin{cases} \bar{P}_i^d = P_i^{dn} \\ \bar{Q}_i^d = Q_i^{dn} \\ \bar{V}_i^d = V_i^{dn} \end{cases} \tag{38}$$

where P_i^{dn} and Q_i^{dn} are the phase-to-neutral active power and reactive power, respectively; and $\bar{P}_i^d$, $\bar{Q}_i^d$, and $\bar{V}_i^d$ are the phase-to-ground active power, reactive power, and voltage magnitude, respectively.

Based on the results obtained by Method I that employs the actual measurement as inputs for PF calculation, the maximum absolute error and the maximum relative error at bus i are defined as (39). In addition, the relative error of the power loss (MRE_{pl}) can also be calculated by (38), and the x_i^d in (39) is replaced by the power loss.

$$\begin{cases} MAE_{x,i} = \max\left| x_i^d - x_{i,\text{Method I}}^d \right| \\ MRE_{x,i} = \dfrac{\max\left| x_i^d - x_{i,\text{Method I}}^d \right|}{x_{i,\text{Method I}}^d} \times 100\% \end{cases} \tag{39}$$

where x_i^d is the voltage magnitude or angle; and $x_{i,\text{Method I}}^d$ is the voltage magnitude or angle calculated by Method I, $x \in \{v,\theta\}$.

2) Grounding Resistance of Slack Bus

The grounding resistance in MVDS ranges from 0 to 20 Ω, and the details are shown in Table VII. R_g represents the setting of the grounding resistance parameter. Under eight settings of R_g, the influence of the modification of the measurement on the PF result is demonstrated. The PF results of Method I are regarded as the benchmark, and the maximum absolute error of voltage magnitude (MAE_v) at each bus of the other three methods are shown in Fig. 4. Furthermore, the varying trend of the neutral point voltage (V_n) at the grounded bus 1 can be investigated from Fig. 4.

TABLE VII
SETTING OF INFLUENCING FACTORS

Factor	Setting number	Parameter
R_g	1-8	[0.001, 4, 8, 10, 13, 15, 18, 20]Ω
SL	1-8	[0.415, 1, 3, 5, 7, 9, 10, 20]×10^{-5} S/mile
VP	1-3	[1, 1, 1]p.u., [1.01, 1, 1]p.u., [1.01, 0.98, 1]p.u.
LR	1-8	[100, 110, 120, 130, 140, 150, 160, 170]%
RE	1-8	[40, 80, 100, 130, 150, 170, 200, 220]%

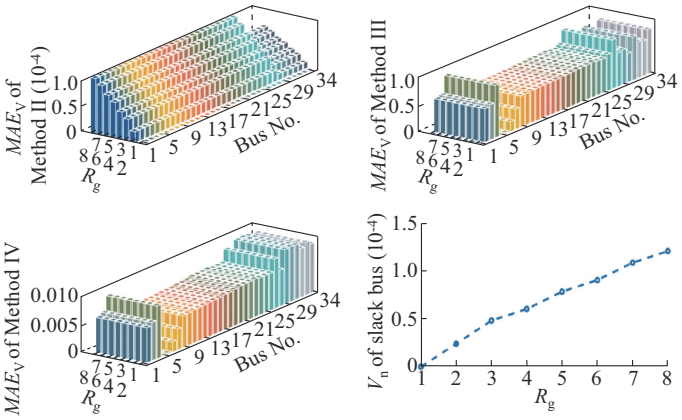

Fig. 4. MAE_v of three methods and V_n of Method I with different R_g.

The MAE_v of Method II increases along with the growth of R_g because this method ignores the V_n at the grounded bus 1. As the R_g increases, the V_n of bus 1 increases. The maximum of V_n is 0.00012 p.u.. The MAE_v of Method III is similar to the MAE_v of Method IV, and the MAE_v of these two methods is much bigger than that of Method II. The different R_g has little influence on the results of Method III and Method IV. The MAE_v of the last two methods is about 0.01 which indicates the poor accuracy of PF calculation. This phenomenon indicates that the error due to the modification of the measurement is greater than the error due to the neglect of the grounded slack bus model under different grounding resistances, but both of them need to be considered.

3) Line Susceptance

The susceptance of the cable is large, which is one of the factors affecting the V_n of bus 1. The settings of the susceptance of lines are shown in Table VII and the R_g is 20 Ω. SL represents the setting of the line susceptance parameter. Under eight settings of SL, the influence of the modification of the measurement on the PF result is demonstrated and the values of MAE_v at each bus of the three methods are shown in Fig. 5. Method II uses the same PF equation as Method I, so the MAE_v of Method II is smaller than that of the other methods in Fig. 5. The maximum values of MAE_v of the three methods are 1.94×10^4, 1.25×10^2, 1.29×10^2, respectively. Different SL has a marginal influence on the MAE_v of the Methods II, III, IV. The varying trend of V_n at bus 1 is shown in Fig. 5. Under the same R_g, along with the increase of SL, the V_n of bus 1 is higher.

4) Voltage Control of Slack Bus

The voltage control will affect the V_n and the settings of voltage magnitude are shown in Table VII. VP represents the

setting of the voltage control. The influence of the modification of the measurement and the slack bus model is demonstrated, and the values of MAE_v at each bus of the three methods are shown in Fig. 6. Compared with different values of R_g and SL, the voltage unbalance of bus 1 has a greater effect on the calculation accuracy of Method III and Method IV. Different VP makes the MAE_v of the three methods change little, and the maximum MAE_v are 1.24×10^{4}, 1.89×10^{2}, 1.98×10^{2}, respectively. The varying trend of V_n at bus 1 is shown in Fig. 6. Under the same R_g and SL, V_n of bus 1 increases with the increase of voltage unbalance. Method IV does not take into account the measurement characteristics and the grounding slack bus model of MVDS, leading to the worst result. Thus, it is necessary to consider the measurement characteristics in the PF equations.

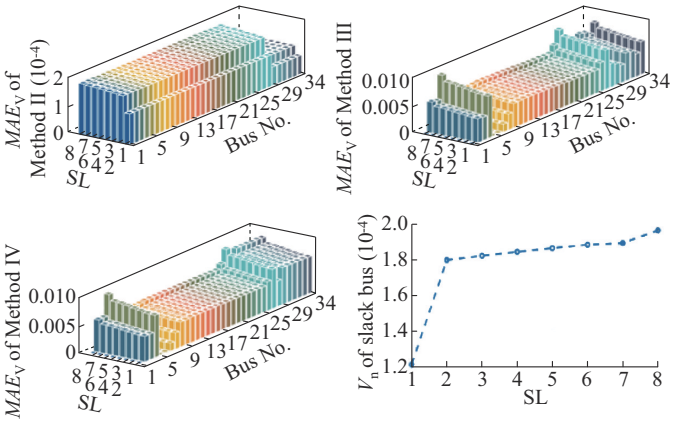

Fig. 5. MAE_v of three methods and V_n of Method I with different SL.

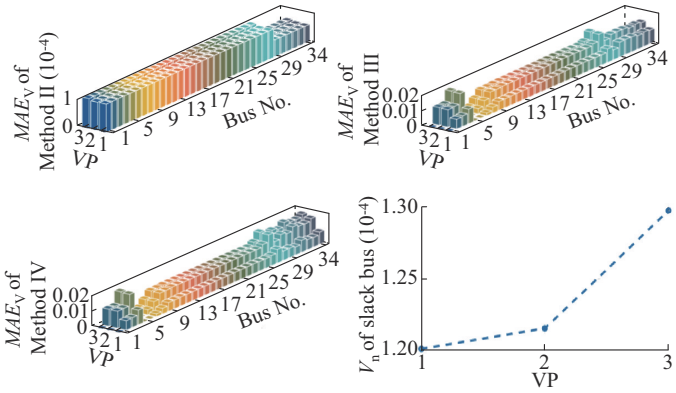

Fig. 6. MAE_v of three methods and V_n of Method I with different VP.

5) Unsymmetrical Load

Unsymmetrical load is a major feature of MVDS. Eight settings of load are used for observing the maximum absolute error of the three methods relative to Method I. LR represents the setting of the load. The parameters of LR in Table VII mean that S_2^{ac}, S_3^{ac}, S_{29}^{an}, S_{29}^{bn}, S_{30}^{an}, and S_{30}^{bn} increase from 100% of its original load to 170%. The MAE_v at each bus of the three methods hardly changes with different loads, and it is similar to the result under different SL. The maximum relative error of voltage angle (MRE_θ) of the three methods are demonstrated in Fig. 7. The values of MRE_θ of Method III and Method IV increase when the load becomes more unbalanced, and the maximum values of MRE_θ of these two methods are 17.82% and 23.92%. It can be drawn from the results that the more the measurement modification is conducted, the more significant MRE_θ will be.

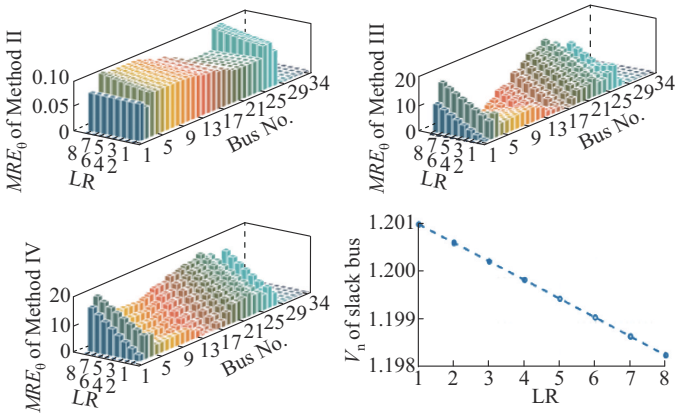

Fig. 7. MRE_θ of three methods and V_n of Method I with different LR.

6) Line Reactance/Resistance Ratio

The line reactance/resistance ratio of MVDS is usually smaller than that of the transmission network. RE represents the setting of the line resistance. The parameters of RE in Table VII represent the line resistance percentage relative to the original value. Under eight settings of RE, the influence of the improvements proposed in this paper is demonstrated. The ranges of the MAE_v of the three methods relative to Method I are similar to those of the result under different SL. The MRE_θ at each bus of the three methods and the varying trend of V_n at bus 1 of Method I are observed in Fig. 8.

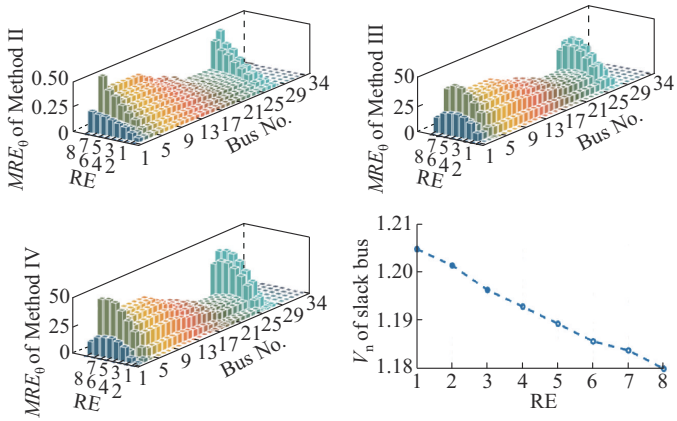

Fig. 8. MRE_θ of three methods and V_n of Method I with different RE.

Obviously, the smaller the RE is, the larger MRE_θ of the three methods are. The impact of RE on the MRE_θ of the three methods is greater than that of LR. The maximum MRE_θ of Method III is 41.11%. The PF result of Method IV is worse as its maximum MRE_θ is 46.92%. The difference between the results of Method III and Method IV illustrates that the measurement characteristics of THM and the transformer model can not be simplified, or else it causes an error of 5.81% in MRE_θ.

7) Security and Economy Analysis

Under different R_g, SL, VP, LR, and RE, the maximum

MRE of voltage magnitude (MRE_v) and MRE_{pl} of the three methods are shown in Table VIII and Table IX. The voltage magnitude error is acceptable within 2% [26]. The maximum MRE_v of Method III is 2.0578 when the line resistance is high. The maximum MRE_v of Method IV exceeds 2% under different LR and RE. The results of the methods from other references that do not consider the measurement characteristics can not accurately reflect the voltage quality in the security analysis.

TABLE VIII
THE MAXIMUM MRE_v IN DIFFERENT CASES

Method	R_g (%)	SL (%)	VP (%)	LR (%)	RE (%)
II	0.0121	0.0200	0.0127	0.0345	0.0423
III	1.0225	1.1248	1.6847	1.9644	2.0578
IV	1.3499	1.2875	1.9665	2.2114	2.4123

TABLE IX
THE MAXIMUM MRE_{pl} IN DIFFERENT CASES

Method	R_g (%)	SL (%)	VP (%)	LR (%)	RE (%)
II	0.13	0.18	0.13	0.18	0.19
III	19.12	25.57	34.17	15.47	25.21
IV	21.09	26.02	37.89	20.21	37.91

The PF model directly influences the calculation and analysis of power loss [27]. According to the PF results, the power company takes measures to reduce the loss and find the location of abnormal line loss. The maximum MRE_{pl} of Method III or Method IV is greater than 15% under any of these factors, which indicates that these two methods are not effective for economy analysis in some situations.

8) Control Characteristics

The bus 4 is considered an equivalent power supply, and its test parameters and control schemes are shown in Table X. This part mainly tests whether the model confirms the control characteristics. The voltage qualification rate β is the ratio of the number of nodes, whose voltage magnitudes are between 0.95 p. u. and 1.05 p. u., to the total number of nodes. The voltage unbalance degree can be quantified by the voltage unbalance coefficient ε which can be formulated as (40).

TABLE X
TEST PARAMETERS AND CONTROL SCHEMES

Test condition	Parameter
Slack bus	$U_a=U_b=U_c=1.0$ p.u.
Control scheme B1	$U_{ac}=U_{bc}=\sqrt{3}\times0.98$ p.u., $P_{ac}=150$ kW, $P_{bc}=150$ kW
Control scheme B2	$U_{ac}=\sqrt{3}\times0.95$ p.u., others the same as B1
Control scheme B3	$U_{ac}=U_{bc}=\sqrt{3}\times0.95$ p.u., others the same as B1
Control scheme B4	$P_{ac}=200$ kW, $P_{bc}=180$ kW, others the same as B1

$$\varepsilon=\frac{\max\left\{\left|U_i^{a}-\bar{U}_i\right|,\left|U_i^{b}-\bar{U}_i\right|,\left|U_i^{c}-\bar{U}_i\right|\right\}}{\bar{U}_i} \tag{40}$$

where $\bar{U}_i$ is the average voltage magnitude of the three phases; and U_i^d is the voltage magnitude, $d\in\{a,b,c\}$.

For the four schemes, the voltage magnitude of each phase is shown in Fig. 9, which also shows the voltage unbalance coefficient of each bus. The power loss rate, voltage qualification rate, and iteration number are shown in Table XI. Accordingly, there is a short summary below.

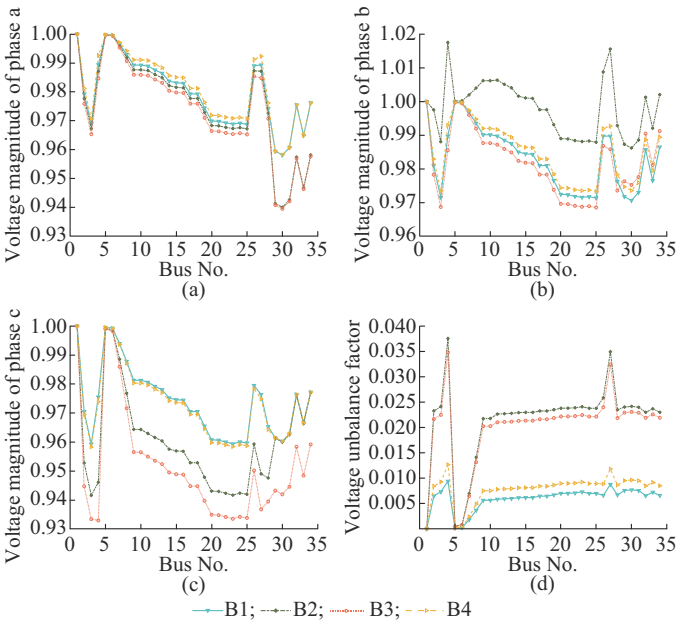

Fig. 9. Voltage magnitudes and voltage unbalance factor of each bus for four control schemes. (a) Voltage magnitude of phase a. (b) Voltage magnitude of phase b. (c) Voltage magnitude of phase c. (d) Voltage unbalance factor.

TABLE XI
TEST RESULTS OF FOUR CONTROL SCHEMES

Control scheme	Power loss rate (%)	β (%)	Iteration time
B1	5.09	100.00	3
B2	8.11	85.29	3
B3	10.18	75.49	4
B4	5.53	100.00	3

1) Based on scheme B1, scheme B2 decreases the phase-to-phase voltage magnitude U_{ac}. The voltage magnitudes U_a and U_c of the buses in the TTN decrease. In scheme B3, U_a, U_b, and U_c of the buses in the TTN decrease. Scheme B4 increases the phase-to-phase active power P_{ac} and P_{bc}, which results in the increase of U_a of the buses in the TTN. Besides, U_b of all buses is higher.

2) Compared with scheme B1, the other schemes adjust the control strategy of bus 4, and ε of all buses is changed. The ε of most buses increases (such as buses 7-27), and the voltage unbalance coefficient curves of schemes B2 and B3 are similar when the voltage magnitude decreases. The power loss rate of scheme B2 is increased from 5.09% to 8.11%, and the voltage qualification rate is reduced from 100% to 85.29%. The main reason for the increase in the power loss rate is the voltage unbalance. The unbalance degree of

scheme B3 becomes higher, and the power loss rate is increased from 5.09% to 10.18%. Moreover, the number of iterations grows as well.

C. Performance Test with High-dimension Networks

1) Test System

A test system of MVDS is designed based on the IEEE 123-bus system [28]. Figure 10 is a single-line diagram of the modified IEEE 123-bus test system. The test conditions and measurements are shown in Appendix A and a description of this test system is summarized in Table XII. Since the PF model of the step voltage regulators can be found in [29], it will not be described in detail in this paper.

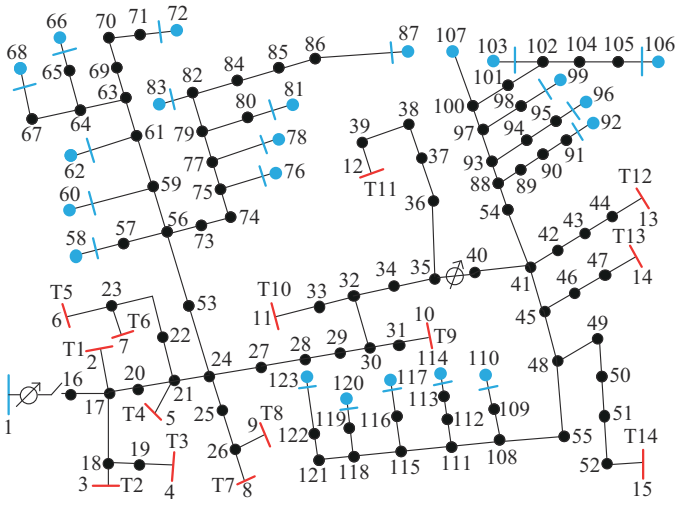

Fig. 10. Single-line diagram of modified IEEE 123-bus test system.

TABLE XII
SYSTEM PARAMETERS OF MODIFIED IEEE 123-BUS TEST SYSTEM

Element	System parameter
Slack bus	Bus 1
Grounding resistance of slack bus	20 Ω
Bus in TFN	Blue buses
Bus in TTN	Black buses
Blue short line measured via THM	Δ/Yn-1 type transformer
Red short line measured via TWM	Transformer ignoring loss
Equivalent load	Blue buses and buses 2-13
Equivalent power supply	Buses 14, 15
Connection bus	Black buses
Step voltage regulator	Circle with arrows

2) Computational Efficiency

For illustrating the computational efficiency of the proposed PF model, Method III and Method IV which belong to commonly used methods in other references are selected for comparison. Based on the modified IEEE 123-bus test system, three influencing factors SL, LR, and RE are selected for analysis and four settings (1/3/5/7) of these factors are used, which can be found in Table VII in Section V-B.

The maximum MRE_v of Method III and Method IV under the four settings of three influencing factors are shown in Table XIII. It can be seen that the maximum values of MRE_v of Method III and Method IV become larger with the increase of buses. The maximum increments of the maximum MRE_v of Method III are 1.1%, 2.66%, and 3.21% under the factors SL, LR, and RE, respectively. The maximum increments of the maximum MRE_v of Method IV are 1.03%, 5.2%, and 2.99% under the factors SL, LR, and RE, respectively. The results show that the methods from other references that do not consider the measurement and structural characteristics will introduce greater PF errors with the increase of system scale.

TABLE XIII
THE MAXIMUM MRE_v FOR FOUR SETTINGS (1/3/5/7) OF DIFFERENT FACTORS

Method	The maximum MRE_v (%)		
	SL	LR	RE
III	2.21/2.21/2.22/2.22	2.21/2.26/2.93/4.62	0.54/1.50/3.46/5.27
IV	2.32/2.32/2.32/2.32	2.32/3.10/5.47/7.41	0.65/1.59/3.58/5.40

The convergence iteration times and the simulation time of the three methods under the four settings of three factors are shown in Table XIV and Table XV. With the increase of SL, the difference in the simulation time of the three methods is not significant, and the iteration times of the three methods both is 3. As the LR increases, the iteration times and the simulation time of Method I and Method III increase. This phenomenon indicates that the load asymmetry will affect the iteration times and the simulation time of the PF method. When the setting of LR is 5 or 7, Method III has more iteration times and simulation time than Method I. The reason is that Method III considers the grounding resistance and neutral point voltage at the secondary side of transformers, while the reference voltage for MVDS is the virtual ground voltage at the slack bus. Under different values of LR, the iteration times and the simulation time of Method IV have almost no change. Compared with Method III, Method IV does not consider the grounding resistance and neutral point voltage at the secondary side of transformers. Compared with Method I, Method IV does not consider the load asymmetry introduced by the load measured via TWM. From the results and analysis of Method IV, the load asymmetry has little impact on the simulation time and a significant impact on the PF error. As the X/R ratio decreases, the iteration times and the simulation time of the three methods increase. It is easy to find that the more iteration times, the longer the simulation time. Compared with the other two methods, Method III is not easy to converge in some cases.

TABLE XIV
ITERATION TIMES FOR FOUR SETTINGS (1/3/5/7) OF DIFFERENT FACTORS

Method	Iteration times		
	SL	LR	RE
I	3/3/3/3	3/4/4/5	3/3/3/4
III	3/3/3/3	3/4/5/6	3/3/4/4
IV	3/3/3/3	3/3/3/3	3/3/3/4

Under different influencing factors, the difference in the simulation time for each iteration of each method lies in the modeling of PF components and the number of PF equations. The three methods are all solved by Newton's method, so the computational efficiency majorly depends on the number of nonlinear equations (i.e., the dimension of the Jacobian matrix). Assume that the number of buses in the TTN is n and the number of buses in the TFN is m. The numbers of nonlinear equations in Method I, Method III, and Method IV are $7+6n+8m$, $6n+8m$, and $6n+6m$, respectively. The number of nonlinear equations in Method I is 7 more than that in Method III. Compared with the number of nonlinear equations for the distribution systems, 7 is small. The number of nonlinear equations in Method I is $7+2m$ more than that in Method IV. With the increase in the number of buses in the TFN, the gap will become significant. In addition, the load asymmetry and the X/R ratio of lines will affect the iteration times and simulation time of the PF model.

TABLE XV
SIMULATION TIME FOR FOUR SETTINGS (1/3/5/7) OF DIFFERENT FACTORS

Method	Simulation time (s)		
	SL	LR	RE
I	7.5/7.4/7.5/7.7	7.6/9.8/9.8/12.3	7.7/7.4/7.4/9.9
III	7.5/7.5/7.6/7.6	7.9/10.3/12.8/14.9	7.8/7.8/10.3/10.3
IV	7.4/7.5/7.4/7.6	7.5/7.6/7.6/7.6	7.7/7.7/7.6/9.7

From the above discussion, it can be seen that the PF error introduced by Method III and Method IV can not be ignored and will directly affect the operation analysis of MVDS. The difference in simulation time between Method I and the other two methods is not significant, and Method I has a better overall performance.

VI. CONCLUSION

Existing research works on the three-phase PF model have some limitations in that they do not use the measurements or the predicted data from SCADA to be the inputs of PF calculation. Therefore, most of them can not be widely applied in the PF calculation for MVDS in practice. An improved three-phase PF method is proposed in this paper, which works based on the PF equations that are suitable for the measurements obtained from THM and TWM. Furthermore, not only the proposed ungrounded slack bus model but also the general model for six types of transformers are incorporated into the proposed PF model.

The comprehensive test results indicate that the general transformer model is more accurate for the PF calculation, and it is feasible for programming. The modified IEEE 34-bus test system is used to show the applicability of the improved three-phase PF method. The differences in the results of various PF models are analyzed from seven different aspects, including grounding resistance, line susceptance, voltage control, unsymmetrical load, line reactance/resistance ratio, security and economy analysis, and control characteristics. Besides, the characteristics of the V_n at the slack bus are also demonstrated in some aspects. The results verify that the proposed model, which treats the conventional measurements as inputs, reduces the error with respect to the models which use the modified measurements. This improved model reflects the control characteristics of the MVDS and leads to more accurate security and economic analysis. The modified IEEE 123-bus test system is used to analyze the computational efficiency of the improved method. Last but not least, the proposed model is effective to be widely used for online PF calculation and works as the basis for the optimal power flow.

APPENDIX A

The load measurements and test conditions of the modified IEEE 34-bus test system are shown in Table AI and Table AII, respectively. The load measurements and test conditions of the modified IEEE 123-bus test system are shown in Table AIII and Table AIV, respectively.

TABLE AI
LOAD MEASUREMENTS OF MODIFIED IEEE 34-BUS TEST SYSTEM

Bus number	S_{ac}/S_1 (kVA)	S_{bc}/S_2 (kVA)	S_3 (kVA)
2	55.78–j18.94	44.24+j10	
3	117.34–j27.91	82.72+j87.68	
29	100+j70	100+j70	100+j70
30	135+j105	135+j105	135+j105
31	80+j20	80+j20	80+j20
32	100+j50	100+j50	100+j50
33	100+j65	100+j65	100+j65
34	50+j10	50+j10	50+j10

TABLE AII
TEST CONDITIONS OF MODIFIED IEEE 34-BUS TEST SYSTEM

Test condition	Parameter
Slack bus	$U_{an}=U_{bn}=U_{cn}=1.0$ p.u.
Bus 4	$U_{ac}=U_{bc}=\sqrt{3}\times0.98$ p.u., $P_{ac}=190.48$ kW, $P_{bc}=109.67$ kW

TABLE AIII
LOAD MEASUREMENTS OF MODIFIED IEEE 123-BUS TEST SYSTEM

Bus number	S_{ac}/S_1 (kVA)	S_{bc}/S_2 (kVA)	S_3 (kVA)
2-13	10+j5	10+j5	
Bus in TFN	5+j1	5+j1	5+j1

TABLE AIV
TEST CONDITIONS OF MODIFIED IEEE 123-BUS TEST SYSTEM

Test condition	Parameter
Slack bus	$U_{an}=U_{bn}=U_{cn}=1.0$ p.u.
Buses 14, 15	$U_{ac}=U_{bc}=\sqrt{3}$ p.u., $P_{ac}=2$ kW, $P_{bc}=2$ kW

REFERENCES

[1] J. E. Fleckenstein, *Calculating and Measuring Power in Three Phase Circuits*, 2nd ed. Fairfax: PDHonline Course, 2013.
[2] K. Tang, S. Dong, J. Shen *et al*., "A robust and efficient two-stage algorithm for power flow calculation of large-scale systems," *IEEE Transactions on Power Systems*, vol. 34, no. 6, pp. 5012-5022, Nov. 2019.

[3] H. Cui, F. Li, and X. Fang, "Effective parallelism for equation and jacobian evaluation in large-scale power flow calculation," *IEEE Transactions on Power Systems*, vol. 36, no. 5, pp. 4872-4875, Sept. 2021.
[4] P. Garcia, S. Cameiro, J. Pereira *et al*., "Three-phase power flow calculations using the current injection method," *IEEE Transactions on Power Systems*, vol. 15, no. 2, pp. 1452-1453, May 2000.
[5] N. Yang, "Three-phase power flow calculations using direct Z_{BUS} method for large-scale unbalanced distribution networks," *IET Generation, Transmission & Distribution*, vol. 10, no. 4, pp. 1048-1055, Mar. 2016.
[6] I. Dzafic, H. Neisius, M. Gilles *et al.*, "Three-phase power flow in distribution networks using Fortescue transformation," *IEEE Transactions on Power Systems*, vol. 28, no. 2, pp. 1027-1034, May 2013.
[7] M. Abdel-Akher, K. M. Nor, and A. H. A. Rashid, "Improved three-phase power-flow methods using sequence components," *IEEE Transactions on Power Systems*, vol. 20, no. 3, pp. 1389-1397, Apr. 2017.
[8] T. Alinjak, I. Pavić, and K. Trupinic, "Improved three-phase power flow method for calculation of power losses in unbalanced radial distribution network," in *Proceedings of 24th International Conference & Exhibition on Electricity Distribution*, Glasgow, UK, Jun. 2017, pp. 2361-2365.
[9] P. Wirasanti and E. Ortjohann, "3-phase 4-wire hybrid calculation – analysis method for clustering power systems philosophy," in *Proceedings of 2015 IEEE Eindhoven PowerTech*, Eindhoven, Netherland, Jun. 2015, pp. 1032-1038.
[10] M. J. E. Alam, K. M. Muttaqi, and D. Sutanto, "A three-phase power flow approach for integrated 3-wire MV and 4-wire multigrounded LV networks with rooftop solar PV," *IEEE Transactions on Power Systems*, vol. 28, no. 2, pp. 1728-1737, May 2013.
[11] T. Alinjak, I. Pavić, and M. Stojkov, "Improvement of backward/forward sweep power flow method by using modified breadth-first search strategy," *IET Generation, Transmission & Distribution*, vol. 11, no. 1, pp. 102-109, Jun. 2017.
[12] X. Zhou, D. Huang, J. Liu *et al*., "Three-phase power flow model of low-voltage distribution network considering phase asymmetry and photovoltaic access," in *Proceedings of 2019 IEEE Sustainable Power and Energy Conference* (*iSPEC)*, Beijing, China, Nov. 2019, pp. 1438-1443.
[13] D. R. R. Penido, L. R. Araujo, C. Sandoval *et al*., "Three-phase power flow based on four-conductor current injection method for unbalanced distribution networks," *IEEE Transactions on Power Systems*, vol. 23, no. 2, pp. 494-503, May 2008.
[14] L. Luo, X. Zhao, W. Yan *et al*., "Improved three-phase power flow model for ungrounded distribution network considering controllability of line-to-line voltage," *Automation of Electric Power Systems*, vol. 41, no. 11, pp. 92-98, Jun. 2017.
[15] W. Yan, H. Yang, X. Zhao *et al*., "Three-phase power flow model for ungrounded distribution networks," *Proceedings of the CSEE*, vol. 33, no. 19, pp. 135-141, Jun. 2013.
[16] J. Suonan, W. Fu, W. Liu *et al*., "Study on power flow algorithm for ungrounded distribution networks," *Proceedings of the CSEE*, vol. 26, no. 10, pp. 86-91, Apr. 2006.
[17] T. A. P. Beneteli, D. R. R. Penido, and L. R. de Araujo, "A new synchronous DG model for unbalanced multiphase power flow studies," *IEEE Transactions on Power Systems,* vol. 35, no. 1, pp. 803-813, Jan. 2020.
[18] M. Coppo, F. Bignucolo, and R. Turri, "Generalised transformer modelling for power flow calculation in multi-phase unbalanced networks," *IET Generation, Transmission & Distribution*, vol. 11, no. 15, pp. 3843-3852, Oct. 2017.
[19] M. R. Irving and A. K. Al-Othman, "Admittance matrix models of three-phase transformers with various neutral grounding configurations," *IEEE Transactions on Power Systems*, vol. 18, no. 3, pp. 1210-1212, Apr. 2003.
[20] W. Wu and B. Zhang, "Derivation of detailed transformer models and three-phase power flow for distribution system," *Automation of Electric Power Systems*, vol. 27, no. 4, pp. 53-56, Feb. 2003.
[21] I. Dzafic, R. A. Jabr, and H. Neisius, "Transformer modeling for three-phase distribution network analysis," *IEEE Transactions on Power Systems*, vol. 30, no. 5, pp. 2604-2611, Sept. 2015.
[22] S. S. Moorthy and D. Hoadley, "A new phase-coordinate transformer model for Ybus analysis," *IEEE Transactions on Power Systems*, vol. 17, no. 4, pp. 951-956, Nov. 2002.
[23] S. Dutto, G. Masetti, S. Chiaradonna *et al*., "On extending and comparing Newton-Raphson variants for solving power-flow equations," *IEEE Transactions on Power Systems*, vol. 34, no. 4, pp. 2577-2587, Jul. 2019.
[24] I. Molina-Moreno, A. Medina, R. Cisneros-Magaña *et al*., "Enhanced harmonic state estimation in unbalanced three-phase electrical grids based on the Kalman filter and physical scale-down implementation," *International Journal of Electrical Power & Energy Systems*, vol. 123, pp. 106243-106252, Jun. 2020.
[25] Y. Yao, X. Liu, D. Zhao *et al*., "Distribution system state estimation: a semidefinite programming approach," *IEEE Transactions on Smart Grid*, vol. 10, no. 4, pp. 4369-4378, Jul. 2019.
[26] *IEEE Recommended Practice for Monitoring Electric Power Quality*, IEEE Standard 1159, 2019.
[27] D. Wang, F. Zhou, and J. Li, "Cloud-based parallel power flow calculation using resilient distributed datasets and directed acyclic graph," *Journal of Modern Power Systems and Clean Energy*, vol. 7, no. 1, pp. 65-77, Jan. 2019.
[28] M. Bazrafshan and N. Gatsis, "Comprehensive modeling of three-phase distribution systems via the bus admittance matrix," *IEEE Transactions on Power Systems*, vol. 33, no. 2, pp. 2015-2029, Mar. 2018.
[29] E. E. Pompodakis, G. C. Kryonidis, and M. C. Alexiadis, "A comprehensive three-phase step voltage regulator model with efficient implementation in the *Z*-bus power flow," *Electric Power Systems Research*, vol. 199, pp. 107443-107454, Jul. 2021.

Zhengmei Lu is currently pursuing the Ph. D. degree with the School of Electrical Engineering, Chongqing University, Chongqing, China. Her research interests include power flow calculation, state estimation, and operation planning for AC/DC distribution networks.

Wei Yan received the Ph.D. degree in electrical engineering from Chongqing University, Chongqing, China, in 1999. Currently, he is a Professor in the School of Electrical Engineering at Chongqing University. His research interests include optimal operation and control in power systems.

Dezhi Huang received the M. S. degree in electrical engineering from Chongqing University, Chongqing, China, in 2020. He is currently working in the State Grid Zhejiang Yiwu Power Supply Company, Yiwu, China. His research interests include state estimation and power flow calculation of power system.

Junjie Tang received the Ph.D. degree in electrical engineering from the Institute for Automation of Complex Power Systems, E.ON Energy Research Center, RWTH Aachen University, Aachen, Germany, in 2014. He is currently an Associate Professor with the Power and Energy Reliability Research Center, State Key Laboratory of Power Transmission Equipment & System Security and New Technology, School of Electrical Engineering, Chongqing University, Chongqing, China. His research interests include complex power system uncertainty quantification analysis, modeling of hybrid AC/DC grid, and application of machine learning in power systems.

Ferdinanda Ponci received the Ph.D. degree in electrical engineering from the Politecnico di Milano, Milano, Italy, in 2002. In 2003, she joined the Department of Electrical Engineering, University of South Carolina, Columbia, USA, as an Assistant Professor, where she became an Associate Professor, in 2008. In 2009, she joined the E.ON Research Center, Institute for Automation of Complex Power Systems, RWTH Aachen University, Aachen, Germany, where she is currently a Professor of Monitoring and Distributed Control for Power Systems. She is a Member of the Administration Committee of the IEEE Instrumentation and Measurement Society and the Liaison with IEEE Women in Engineering. Her research interests include monitoring and control of active electrical distribution grids and urban energy grids.

Antonello Monti received the M.Sc. degree (summa cum laude) and the Ph.D. degree in electrical engineering from the Politecnico di Milano, Milano, Italy, in 1989 and 1994, respectively. He started his career with Ansaldo Industria and then moved to the Politecnico di Milano as an Assistant Professor, in 1995. In 2000, he joined the Department of Electrical Engineering, University of South Carolina, Columbia, USA, as an Associate Professor, and then a Full Professor. Since 2008, he has been the Director of the Institute for Automation of Complex Power System with the E.ON Energy Research Center, RWTH Aachen University, Aachen, Germany, and he also holds a joint affiliation with the Digital Energy Fraunhofer FIT, Aachen, Germany. He is the author or coauthor of more than 300 peer-reviewed papers published in international journals and in the proceedings of international conferences. His research interests include automation of complex power system and digital energy.